



## Role of impurities and dislocations for the unintentional n-type conductivity in InN

V. Darakchieva<sup>a,b,c,\*</sup>, N.P. Barradas<sup>a,b</sup>, M.-Y. Xie<sup>c</sup>, K. Lorenz<sup>a,b</sup>, E. Alves<sup>a,b</sup>, M. Schubert<sup>d</sup>, P.O.Å. Persson<sup>c</sup>, F. Giuliani<sup>c</sup>, F. Munnik<sup>e</sup>, C.L. Hsiao<sup>c,f</sup>, L.W. Tu<sup>f</sup>, W.J. Schaff<sup>g</sup>

<sup>a</sup> Instituto Tecnológico e Nuclear, 2686-953 Sacavém, Portugal

<sup>b</sup> CFNUL, 1649-003 Lisboa, Portugal

<sup>c</sup> IFM, Linköping University, SE-581 83 Linköping, Sweden

<sup>d</sup> Department of Electrical Engineering, University of Nebraska, Lincoln, NE 68588, USA

<sup>e</sup> Forschungszentrum Dresden Rossendorf, 01314 Dresden, Germany

<sup>f</sup> Department of Physics and Center for Nanoscience and Nanotechnology, National Sun Yat-Sen University, Kaohsiung 80424, Taiwan, ROC

<sup>g</sup> Department of Electrical and Computer Engineering, Cornell University, Ithaca, NY 14853, USA

### A B S T R A C T

We present a study on the role of dislocations and impurities for the unintentional n-type conductivity in high-quality InN grown by molecular beam epitaxy. The dislocation densities and H profiles in films with free electron concentrations in the low  $10^{17} \text{ cm}^{-3}$  and mid  $10^{18} \text{ cm}^{-3}$  range are measured, and analyzed in a comparative manner. It is shown that dislocations alone could not account for the free electron behavior in the InN films. On the other hand, large concentrations of H sufficient to explain, but exceeding substantially, the observed free electron densities are found. Furthermore, enhanced concentrations of H are revealed at the film surfaces, resembling the free electron behavior with surface electron accumulation. The low-conductive film was found to contain C and it is suggested that C passivates the H donors or acts as an acceptor, producing compensated material in this case. Therefore, it is concluded that the unintentional impurities play an important role for the unintentional n-type conductivity in InN. We suggest a scenario of H incorporation in InN that may reconcile the previously reported observations for the different role of impurities and dislocations for the unintentional n-type conductivity in InN.

© 2009 Elsevier B.V. All rights reserved.

### 1. Introduction

Recent developments in group-III nitride technology have led to the commercialization of a variety of optoelectronic devices with large impact on everyday life. In particular, high-brightness blue and white light emitting diodes based on InGaN promise more efficient lighting solutions [1]. An emerging potential application of InGaN and InAlN alloys is in highly efficient multijunction solar cells [2]. Furthermore, InN and related alloys are promising for developing high-frequency transistors, THz emitters and chemical sensors. Driven by the attractive material applications, the epitaxial techniques to grow InN and related alloys have made significant advances and matured during the last decade. However, the poor understanding of the doping mechanism in InN and the related In-rich alloys is one of the

critical issues that hinder further progress in the InN based technology towards full exploitation of the material potential.

Understanding and controlling doping mechanisms in semiconductors are indispensable for their incorporation into new electronic devices, and challenge scientists to unravel the physics behind the sometimes peculiar free charge carrier generating mechanisms. As a result of its exceptional propensity for n-type doping [3] all unintentionally doped InN is n-type conductive but the exact doping mechanism is under debate [4–10]. Difficulties to assess doping in InN and In rich alloys are encountered because of the presence of electron accumulation at the film surfaces with surface charge densities ranging from  $10^{13}$  to  $3 \times 10^{14} \text{ cm}^{-2}$ . Electrical measurements are dominated by the accumulation layer conductivity, complicating their interpretation, since the exact current paths are difficult to determine. The latter are required in order to assign separately the free-charge carrier densities and mobilities to the individual layers of a sample.

The free electron concentration in InN films measured by single field electrical Hall effect was found to decrease with increasing film thickness. Some models derived on the basis of such electrical measurements favor positively charged  $N$  vacancies,  $V_N^+$  associated

\* Corresponding author at: Instituto Tecnológico e Nuclear, 2686-953 Sacavém, Portugal.

E-mail address: [vanya@itn.pt](mailto:vanya@itn.pt); [vanya@ifm.liu.se](mailto:vanya@ifm.liu.se) (V. Darakchieva).

with dislocations as the major origin of the thickness dependent unintentional bulk doping [5,8]. On the other hand, the electrical Hall effect electron concentrations were also reported to correlate with unintentional impurities, such as H and O [4,7]. Indeed, a recent theoretical study reported lower formation energies and thus higher equilibrium concentrations of H donors ( $H_N^{2+}$  and  $H_i$ ) in comparison with  $V_N$ , suggesting H as the plausible cause of the unintentional doping in InN [9]. We have recently reported also a decrease of the bulk free electron concentration with film thickness measured by the contactless optical Hall effect [10,11]. The variation of the bulk free electron concentration with film thickness, however, does not follow the electrical Hall effect models accounting for a constant background electron concentration and free electrons generated by nitrogen vacancies along dislocations [10,11]. These findings indicated the existence of an additional thickness-dependent doping mechanism and motivate the need of further investigations in view of the existing controversy.

An argument in favor of the native defects as dominant donor species over the unintentional impurities is sometimes the low background impurity concentrations in InN films [8,12]. The latter are often measured by secondary ion mass spectrometry (SIMS), which largely relies on the use of standards and may introduce significant uncertainties in the impurity concentrations. On the other hand, ion beam analysis techniques, such as elastic recoil detection analysis (ERDA), measure directly the impurity concentrations and depth profiles, and can provide valuable insights in this respect. In this work we study the role of dislocations and impurities for the unintentional doping in InN films with bulk free electron concentrations in the low  $10^{17} \text{ cm}^{-3}$  and mid  $10^{18} \text{ cm}^{-3}$  range using a combination of infrared spectroscopic ellipsometry (IRSE), transmission electron microscopy (TEM), X-ray diffraction (XRD) and ERDA.

## 2. Experimental

State-of-the-art unintentionally n-type doped InN films with (0001) orientations and thicknesses of 1.3 and 1.6  $\mu\text{m}$  were grown on sapphire substrates by molecular beam epitaxy (MBE). An in-situ GaN/AlN buffer sequence and a 1- $\mu\text{m}$ -thick GaN template layer grown by MBE were employed for the growth of the thicker (sample A) [13] and thinner (sample B) InN layers [14], respectively.

The free electron properties in the InN films were measured by infrared spectroscopic ellipsometry (IRSE) using a rotating compensator infrared ellipsometer (J.A. Woollam Co., Inc.) in the spectral range of 350–2000  $\text{cm}^{-1}$  with a spectral resolution of 2  $\text{cm}^{-1}$ , and at 60° and 70° angles of incidence. The IRSE data were analyzed by employing anisotropic dielectric functions of sapphire and InN in the model calculations. The sapphire dielectric functions reported in Ref. [15] were used in the data analysis. Contributions of the IR active polar phonons to the InN model dielectric function (MDF) were accounted for by a product presentation of harmonic oscillator lineshapes with Lorentzian broadening [16–18]. The free-carrier contributions were accounted for by the classical Drude model [16–18]. The parameters of the InN MDF and layer thickness were varied until measured and calculated IRSE data simultaneously matched for all spectral data points. As a result, the phonon mode parameters, the high-frequency limit of the dielectric function, the thickness, the free electron concentration and mobility in the InN films have been determined.

Transmission electron microscopy (TEM) specimens were prepared by focused ion beam milling using a Zeiss 1540 EsB cross beam instrument following the lift out technique. The

cross-sectional TEM images were obtained in a FEI Tecnai G2 ultra twin microscope operating at 200 kV.

Elastic recoil detection analysis (ERDA) measurements were performed with 2 MeV  $^4\text{He}^+$  ions at a tilt angle of 78° to measure the H profiles in the films. The spectra were collected with a Schottky barrier detector placed at 24° scattering angle in IBM geometry. To prevent scattered  $^4\text{He}^+$  particles from hitting the ERDA detector, a Kapton foil with a thickness of 8  $\mu\text{m}$  was placed in front of it. In addition, heavy ion (HI) ERDA with a  $^{35}\text{Cl}^{7+}$  35 MeV beam was performed, with backscattered Cl and recoils detected with a Bragg chamber, and H detected simultaneously with a surface barrier Si detector using an Al foil to stop the scattered Cl beam. All data were analyzed with the IBA DataFurnace NDF [19].

X-ray diffraction (XRD) was performed using a Philips triple axis diffractometer with a parabolic graded multilayer mirror collimator, followed by a channel-cut 2-bounce Ge(220) monochromator on the primary side and an asymmetric 2-bounce Ge(220) analyzer [20].

## 3. Results and discussion

Fig. 1 shows scanning electron micrographs of the two InN samples. The surface of the low conductive film A is rather peculiar displaying the presence of craters [indicated by C in Fig. 1(a)], hillocks [indicated by H in Fig. 1(a)] and flat areas [indicated by F in Fig. 1(a)]. The diameters of the craters vary between 1 and 10  $\mu\text{m}$  and the higher magnification image of the hillocks [Fig. 1(a), right panel] reveals that they consist of small crystallites blistering from the surface. Energy dispersive X-ray (EDX) spectra taken from the different areas of film A indicate that the flat areas and the hillocks have similar In content, and no In droplets could be detected in any area type of the film. Very strong EDX Ga signal ( $\sim 50 \text{ at}\%$ ) and negligible In signal in the craters indicate that they most likely extend to the GaN buffer layer. In contrast to film A, the surface morphology of film B is very smooth with fine grain structure [Fig. 1(b)].

Fig. 2 shows experimental and best-model calculated IRSE spectra for the two InN films. The best-model calculated and experimental data are in very good agreement. The InN films were found to be constituted of a bulk, with a lower free electron concentration,  $N_b$  and a thin surface layer (thickness  $d_s$ ) with a higher electron charge accumulation concentration,  $N_s$ . The electron concentration in the GaN buffer layers turned out to be below the detection limit of the IRSE technique, which can be estimated to be approximately  $1 \times 10^{17} \text{ cm}^{-3}$  for n-type GaN [21]. The free electron concentrations extracted from the best-match modeling to the experimental IRSE spectra of the two InN films are summarized in Table 1. The bulk free-electron concentrations,  $N_b$ , (also given above the respective spectra in Fig. 2) are  $1.9 \pm 0.1 \times 10^{17}$  and  $4.71 \pm 0.04 \times 10^{18} \text{ cm}^{-3}$ , respectively. The surface electron sheet densities, provided by the product  $N_s d_s$ , are  $1.0 \pm 0.7 \times 10^{13}$  and  $0.3 \pm 0.1 \times 10^{13} \text{ cm}^{-2}$  for sample A (low conductive) and sample B (highly conductive), respectively. The drastic changes in the IRSE spectra in Fig. 2 are primarily caused by the different bulk free electron concentrations of  $1.9 \times 10^{17}$  and  $4.71 \times 10^{18} \text{ cm}^{-3}$  in the two InN films. For high  $N_b$  values the free electrons effectively screen the polar phonons of sapphire, GaN buffer and InN. Hence, the spectral features due to the  $A_1(\text{LO})$  phonons appear strongly damped. In particular, the large dip in  $\Psi$  for the low conductive film near the InN uncoupled  $A_1(\text{LO})$  phonon at about 594  $\text{cm}^{-1}$  [Fig. 2(a)] vanishes for the film with high  $N_b$  [Fig. 2(b)] due to strong LO-phonon-plasmon coupling [22].

Fig. 3 shows bright field TEM micrographs of the two InN films, recorded with the electron beam parallel to  $\langle 11\bar{2}0 \rangle$ , which

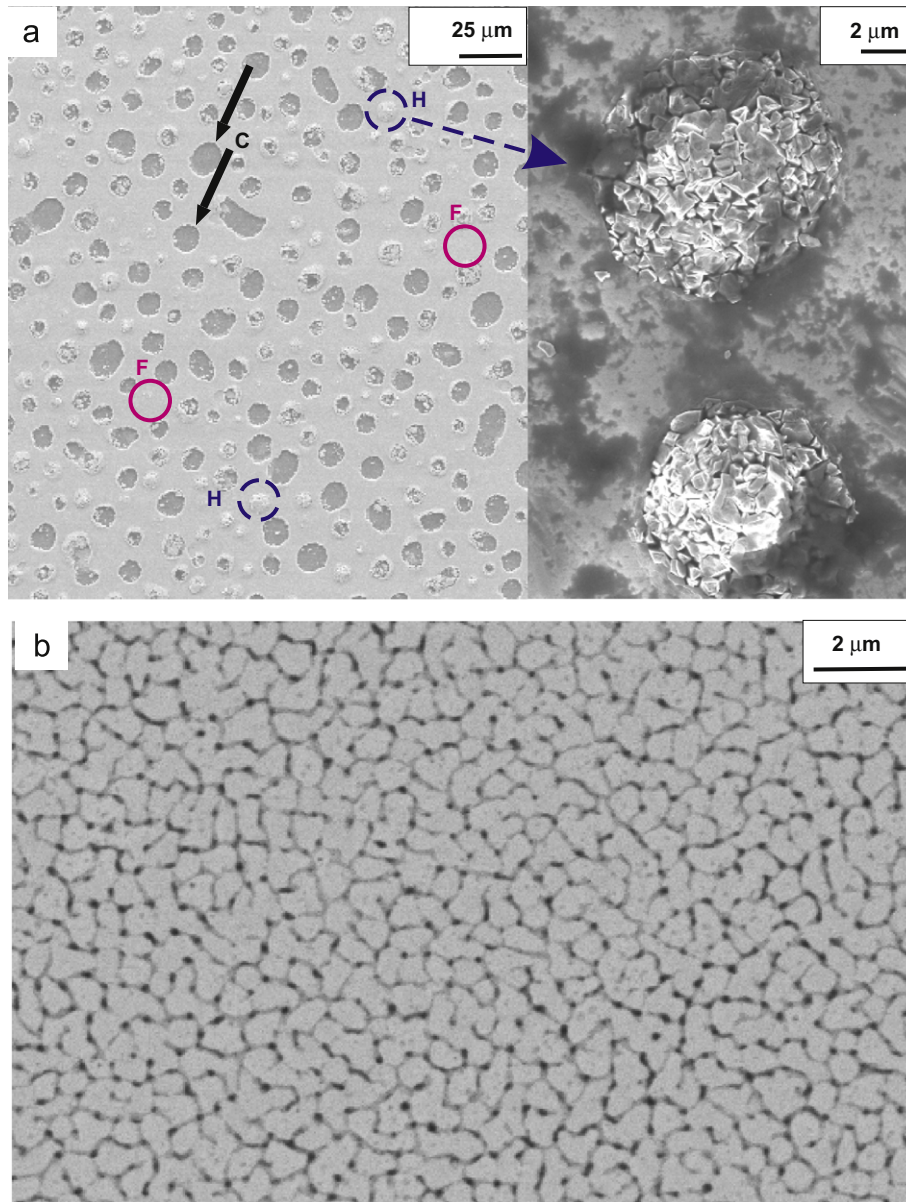


**Fig. 1.** Scanning electron micrographs of the two InN films (a) sample A—InN thickness of 1.6  $\mu\text{m}$  grown on GaN/AlN buffer layer—under two different magnifications and (b) sample B—InN thickness of 1.3  $\mu\text{m}$  grown on MBE GaN template. The morphological features in (a) are indicated as follows: flat areas, F—red circles; hillocks, H—dashed blue circles and craters, C—black arrows. The right panel of (a) shows the hillocks at higher magnification. (For interpretation of the references to the color in this figure legend, the reader is referred to the web version of this article.)

provides contrast with all present threading dislocations. Thin highly defective InN regions ( $\approx 250\text{ nm}$  thick) can be seen at the interface with the GaN buffer layer for both samples [Figs. 3(a) and (b)]. Above the interfacial region the dislocation density is estimated to vary only marginally with film thickness, from  $1.7 \pm 0.2 \times 10^{10}$  to  $0.9 \pm 0.3 \times 10^{10} \text{ cm}^{-2}$  for the InN film in Fig. 3(a) and from  $3.1 \pm 0.1 \times 10^{10}$  to  $2.4 \pm 0.3 \times 10^{10} \text{ cm}^{-2}$  for the InN film in Fig. 3(b) (see also Table 1). These results are in agreement with previous findings that the major change in dislocation density in InN takes place within the substrate/buffer interfacial region of the InN film [23].

The fact that the dislocation density varies only marginally with thickness has also been confirmed separately for screw and edge type dislocations with dark field TEM imaging with different  $\mathbf{g}$ -vectors (not shown here). The dark field TEM images reveal that the film with  $N_b$  of  $4.71 \times 10^{18} \text{ cm}^{-3}$  may contain slightly larger numbers of screw and mixed dislocations compared to edge type

dislocations. On the other hand, the edge type dislocations in the low conductive film are found to be slightly larger in density than dislocations with screw component. To exclude the possibility of any local peculiarities in the dislocation contents we have also estimated the densities of dislocations from XRD. The density of edge dislocations,  $D_e$ , can be estimated from the full width at half maximum of the InN (30 $\bar{3}$ 2) rocking curve,  $\text{FWHM}_{30\bar{3}2}$ , as  $D_e = (1.2\text{FWHM}_{30\bar{3}2})^2 / (4.35b^2)$ , where  $b = 0.57033 \text{ nm}$  [24]. We estimated for our films  $D_e = 1.8 \times 10^{10} \text{ cm}^{-2}$  for the low conductive InN film A and  $N_e = 1.1 \times 10^{10} \text{ cm}^{-2}$  for the highly conductive InN film B, confirming the TEM observations.

The only marginal variation of dislocation densities across our films is in contrast to the large decrease of dislocation densities from low  $10^{11} \text{ cm}^{-2}$  to mid  $10^9 \text{ cm}^{-2}$  range over a thickness of 1–2  $\mu\text{m}$ , previously observed for MBE InN films grown on sapphire using AlN buffer layers [6]. Similar scaling factors for the density of dislocations and bulk electron concentration

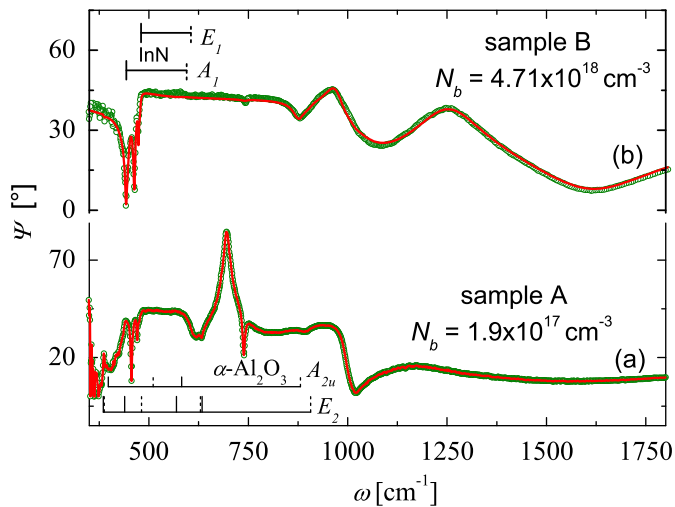


**Fig. 2.** Experimental (circles) and best-model (solid lines) IRSE  $\Psi$  spectra for the InN films with (a) sample A with thickness of  $1.6 \mu\text{m}$  and  $N_b = 1.9 \times 10^{17} \text{ cm}^{-3}$  and (b) sample B with thickness of  $1.3 \mu\text{m}$  and  $N_b = 4.71 \times 10^{18} \text{ cm}^{-3}$ . The bulk,  $N_b$  electron densities are indicated above the respective spectra and the phonon modes of InN and the sapphire substrate are indicated with brackets (solid and dashed lines indicate TO and LO phonons, respectively).

**Table 1**

Best-model IRSE free electron densities, dislocation densities estimated from TEM and XRD, and H and C concentrations for the InN films: bulk free electron concentration,  $N_b$ , surface electron sheet density,  $N_s d_s$ , TEM density of dislocations in the surface,  $D_s$ , and interface region,  $D_i$ , density of edge type dislocations estimated from XRD,  $D_e$ , total amount of surface hydrogen,  $[H]_s$ , bulk hydrogen concentration,  $[H]_b$ , and bulk carbon concentration,  $[C]$ .

Sample	A	B
$N_b$ ( $10^{17} \text{ cm}^{-3}$ )	$1.9 \pm 0.1$	$47.1 \pm 0.5$
$N_s d_s$ ( $10^{13} \text{ cm}^{-2}$ )	$1.0 \pm 0.1$	$0.3 \pm 0.1$
$D_i$ ( $10^{10} \text{ cm}^{-2}$ )	$1.7 \pm 0.2$	$3.1 \pm 0.1$
$D_s$ ( $10^{10} \text{ cm}^{-2}$ )	$0.9 \pm 0.3$	$2.4 \pm 0.3$
$D_e$ ( $10^{10} \text{ cm}^{-2}$ )	1.8	1.1
$H_s$ ( $10^{16} \text{ cm}^{-2}$ )	$4.8 \pm 0.1$	$1.79 \pm 0.03$
$H_b$ (at%)	$0.6 \pm 0.1$	$0.05 \pm 0.03$
C (at%)	$1.0 \pm 0.5$	–

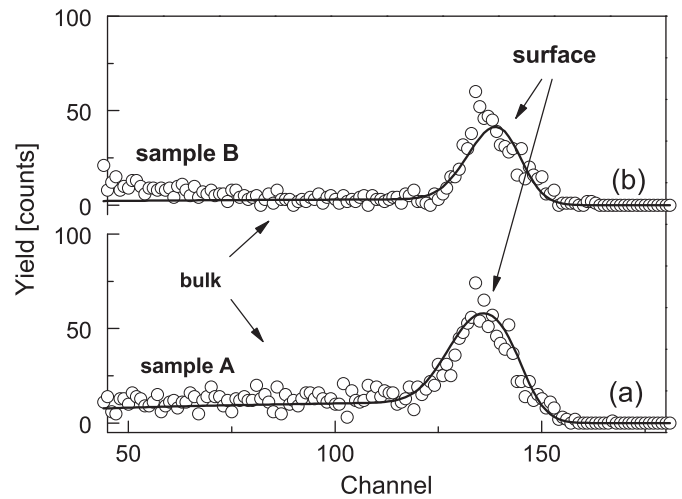


**Fig. 4.** ERDA Hydrogen profiles of (a) sample A and (b) sample B.

measured by electrical Hall effect were also reported in this previous work concluding on the major role of the dislocations for the unintentional n-type conductivity in InN [6,5]. Our present TEM findings of nearly unchanged dislocation density with film thickness indicate that dislocations could not play the dominant role for the thickness dependent unintentional conductivity for our InN grown on GaN buffers or templates, which is in agreement with our previous optical Hall effect observations [10]. More importantly, we find here similar densities of dislocations in InN films with bulk electron concentrations that differ by more than an order of magnitude suggesting that different donor defect(s) unrelated to dislocations must be present. Unintentional impurities, such as H, O and Si are the obvious candidates.

Fig. 4 shows the H profiles measured by  $\text{He}^+$  ERDA in the two InN films. A significant enhancement of the H concentration is observed at the surfaces of the two films. This H profile could match the profile of free electron carriers at the surfaces of the InN samples with large accumulation of electrons. The results were also confirmed by the HI-ERDA and the estimated impurity concentrations are given in Table 1. Note that a higher total amount of H in the surface region is measured for the film with the higher surface sheet density. These observations indicate that H might play an important role for the surface charge properties in InN. High H concentrations of  $0.6 \pm 0.1$  at% and  $0.05 \pm 0.03$  at% are also measured in the bulk of the InN films with  $N_b = 1.9 \times 10^{17} \text{ cm}^{-3}$  (sample A) and  $N_b = 4.71 \times 10^{18} \text{ cm}^{-3}$  (sample B), respectively. It is worth mentioning that we have detected hydrogen in a large number of InN films grown with different surface orientations, thicknesses, doping and at four different growth laboratories and detailed studies on the subject will be reported elsewhere. In all cases the bulk H concentrations are sufficient to explain, but exceed substantially, the bulk electron concentrations. It is possible that part of the H is present in electrically inactive sites or complexes. The enhanced surface concentrations of H measured in the films (Table 1 and Fig. 4) strongly suggest that post growth surface contamination by H is taking place in InN, most probably as a result of the samples exposure to ambient atmosphere. Therefore, certain amount of H could be incorporated in the bulk of the films after growth via diffusion from the near-surface regions. Note that the different surface morphologies (see Fig. 1) may tolerate different H incorporation in the surface regions while the specific film microstructure is expected to affect the diffusion giving rise to rather complex H behavior. Indeed, the total amount of surface hydrogen is much higher in film A with much rougher surface morphology (see Fig. 1 and Table 1). It is also possible that the surface morphology of

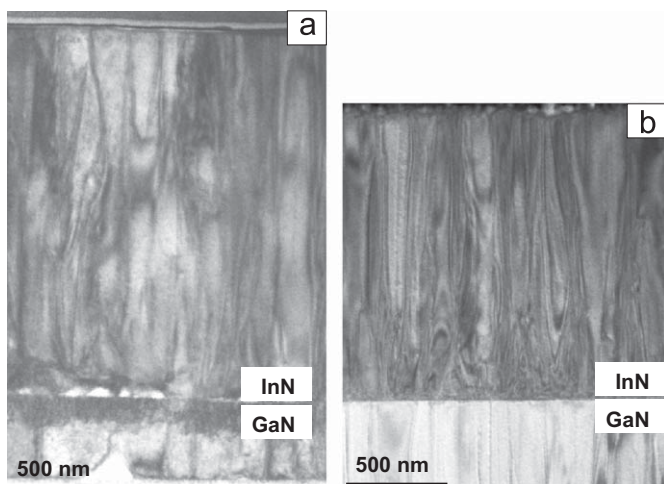


**Fig. 3.** Cross-section bright-field TEM images with the diffraction vector parallel to  $\langle 11\bar{2}0 \rangle$  of (a) sample A and (b) sample B.

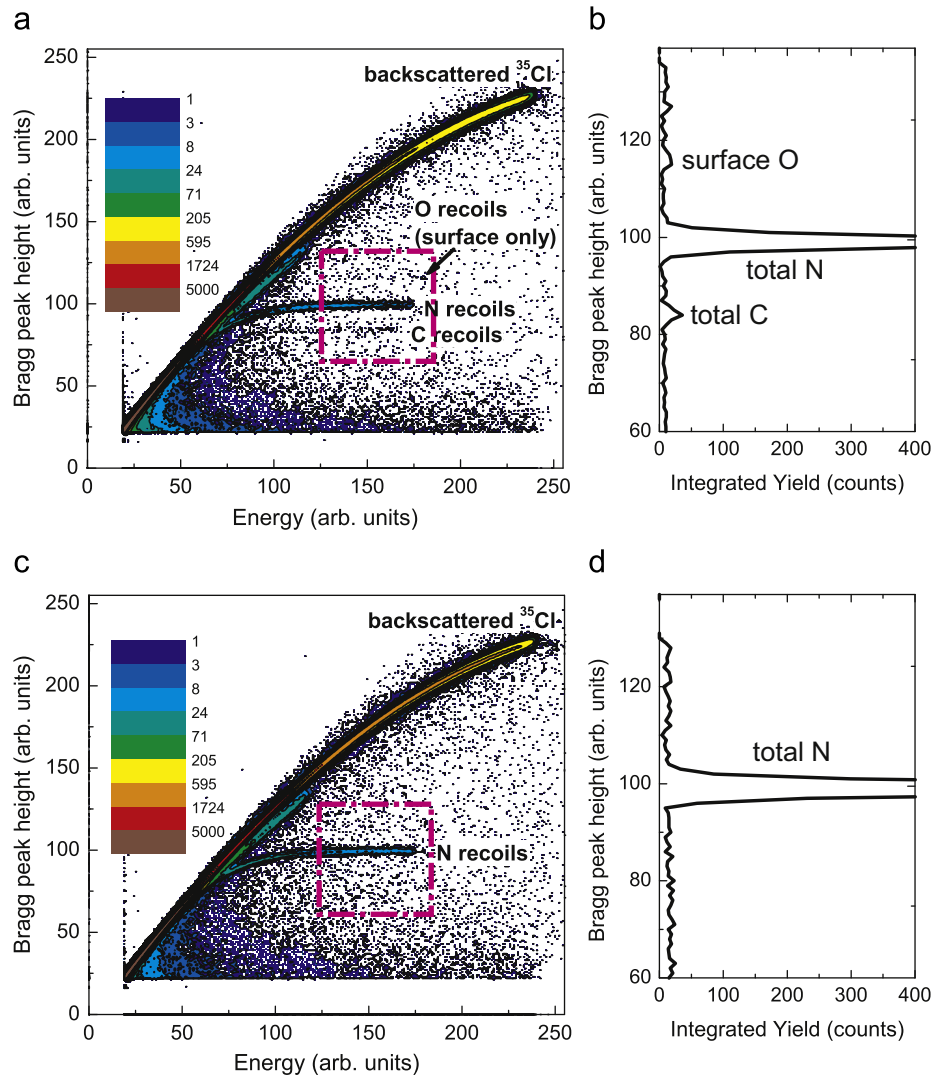


**Fig. 5.** HI-ERDA profiles of (a) sample A and (c) sample B. Integrated yields over the windows indicated in (a) and (c) and projected on the Bragg peak height axes are displayed in (b) and (d) for the A and B films, respectively.

film A is partly a consequence of the large amount of hydrogen in the film, which may provoke blistering.

We note that the scenario of surface H incorporation and subsequent diffusion suggested here may also effectively explain the previously reported different observations for the role of dislocations and impurities for the unintentional n-type conductivity in InN [4–8,10]. Naturally, films grown at similar conditions and nucleation schemes, and having similar sample histories are expected to incorporate similar amounts of hydrogen in the near surface regions. Then the H diffusion in the bulk will be mainly governed by the film microstructure and films with higher densities of dislocations will show higher bulk free electron concentrations. Findings correlating the free electron concentration to dislocation density are reported in Refs. [5,6] and consistent with our scenario. Whenever the InN films are grown at different conditions or/and have different sample histories, such as in the present study, the bulk free electron concentration could no longer be uniquely correlated to the dislocation density. This is also in agreement with our previous Optical Hall effect study of a series of InN films [10,11]. The suggested scenario could also explain previous findings correlating the amounts of H to the free electron concentrations in InN [4,7].

Interestingly, the low conductive film A shows higher amount of H compared to the film B with the higher free electron concentration. We also found that the bulk H concentration varies in different

areas of these films. The HI-ERDA results [Figs. 5(a) and (b)] further show the presence of C impurities in the low-conductive film, estimated to be  $1.0 \pm 0.5$  at%. C may act as an acceptor in InN compensating the H donors and thus explaining the low free electron concentration in this film. Indeed, a recent theoretical study has concluded that substitutional C on the N site,  $C_N$ , has the lowest formation energy and acts as a single acceptor [25]. It is also possible that C forms complexes with H passivating the H donors rather than compensating them. The large electron mobility in film A of  $1600 \text{ cm}^2/(\text{Vs})$  speaks in favor of the latter speculation, however, more work is required to clarify this issue. Some surface O close to the detection limit of 0.5 at% could also be resolved for the low conductive film [Figs. 5(a) and (b)], which in addition will affect the surface charge properties in this case. No additional impurities could be detected in the bulk of the InN films from the HI-ERDA profiles (Fig. 5).

#### 4. Conclusions

The role of dislocations and impurities for the unintentional n-type conductivity in state-of-the-art MBE InN has been studied. TEM investigations, corroborated with XRD, revealed similar densities of dislocations in films with bulk electron

concentrations that differ by more than an order of magnitude. This finding strongly suggests that native defects along dislocations could not play a dominant role for the unintentional n-type doping in MBE InN films grown on GaN buffers or templates. This assertion is further supported by the fact that the dislocation densities change only marginally across the films and thus could not alone explain the previously reported decrease of bulk electron density with increasing film thickness for films grown using similar nucleation schemes. On the other hand, we found significant concentrations of H in the InN films sufficient to explain, but substantially exceeding, the measured bulk electron concentrations. The H profiles revealed enhanced concentrations at the film surfaces, resembling the free electron behavior with surface electron accumulation. Furthermore, a large concentration of C is found in the low conductive film and it is suggested that C acts as an acceptor, in corroboration with a recent theoretical study [25], compensating the H donors or forms complexes with H passivating the H donors in this case. Therefore, it is concluded that unintentional impurities, such as H and C, play an important role for the unintentional n-type conductivity in InN.

### Acknowledgments

VD gratefully acknowledges Prof. B. Monemar for valuable discussions, continuous support, and encouragement. This work is financially supported by FCT Portugal under program Ciência 2007 and contract PTDC/FIS/100448/2008, and by the Swedish Research Council (VR) under contract 2005-5054. The HI-ERDA work is supported by EU-“Research Infrastructures Transnational Access” program AIM “Center for Application of Ion Beams in Materials Research” under EC contract no. 025646. Financial support from NSF MRSEC (DMR-0820521), U.S. Army Research Office (W911NF-08-C-0111), and J.A. Woollam Foundation is acknowledged.

### References

- [1] E.F. Schubert, *Light-emitting Diodes*, Cambridge University Press, Cambridge, UK, 2003.
- [2] L. Hsu, W. Walukiewicz, *J. Appl. Phys.* 104 (2008) 024507.
- [3] W. Walukiewicz, *Physica B* 302 (2001) 123.
- [4] D.C. Look, H. Lu, W.J. Schaff, J. Jasinski, Z. Liliental-Weber, *Appl. Phys. Lett.* 80 (2002) 258.
- [5] V. Cimalla, V. Lebedev, F.M. Morales, R. Goldhahn, O. Ambacher, *Appl. Phys. Lett.* 89 (2006) 172109.
- [6] V. Lebedev, V. Cimalla, T. Baumann, O. Ambacher, F.M. Morales, J.G. Lozano, D. González, *J. Appl. Phys.* 100 (2006) 094903.
- [7] C.S. Gallinat, G. Koblmüller, J.S. Brown, S. Bernardis, J.S. Speck, G.D. Chern, E.D. Readinger, H. Shen, M. Wraback, *Appl. Phys. Lett.* 89 (2006) 032109.
- [8] L.F.J. Piper, T.D. Veal, C.F. McConville, H. Lu, W.J. Schaff, *Appl. Phys. Lett.* 88 (2006) 252109.
- [9] A. Janotti, C.G. Van de Walle, *Appl. Phys. Lett.* 92 (2008) 032104.
- [10] V. Darakchieva, T. Hofmann, M. Schubert, B.E. Sernelius, B. Monemar, P.O.A. Persson, F. Giuliani, E. Alves, H. Lu, W.J. Schaff, *Appl. Phys. Lett.* 94 (2009) 022109.
- [11] T. Hofmann, V. Darakchieva, B. Monemar, H. Lu, W.J. Schaff, M. Schubert, *J. Electron. Mater.* 37 (2008) 611.
- [12] W. Walukiewicz, J.W. Ager III, K.M. Yu, Z. Liliental-Weber, J. Wu, S.X. Li, R.E. Jones, J.D. Denlinger, *J. Phys. D: Appl. Phys.* 39 (2006) R83.
- [13] H. Lu, W.J. Schaff, J. Hwang, H. Wu, G. Koley, L.F. Eastman, *Appl. Phys. Lett.* 79 (2001) 1489.
- [14] C.-T. Liang, Z.H. Sun, C.L. Hsiao, Z.M. Hsu, L.W. Tu, J.-Y. Lin, L.C. Chen, J.H. Chen, Y.F. Chen, C.T. Wu, *Appl. Phys. Lett.* 90 (2007) 172101.
- [15] M. Schubert, T.E. Tiwald, C.M. Herzinger, *Phys. Rev. B* 61 (2000) 8187.
- [16] V. Darakchieva, T. Paskova, M. Schubert, P.P. Paskov, H. Arwin, B. Monemar, D. Hommel, M. Heuken, J. Off, F. Scholz, B.A. Haskell, P.T. Fini, J.S. Speck, S. Nakamura, *Phys. Rev. B* 75 (2007) 195217.
- [17] V. Darakchieva, *Phys. Status Solidi A* 205 (2008) 905.
- [18] M. Schubert, *Infrared Ellipsometry on Semiconductor Layer Structures: Phonons, Plasmons and Polaritons*, vol. 209, Springer, New York, 2004.
- [19] N.P. Barradas, C. Jeynes, R.P. Webb, *Appl. Phys. Lett.* 71 (1997) 291.
- [20] V. Darakchieva, T. Paskova, P.P. Paskov, B. Monemar, N. Ashkenov, M. Schubert, *J. Appl. Phys.* 97 (2005) 013537.
- [21] A. Kasic, M. Schubert, S. Einfeldt, D. Hommel, T. Tiwald, *Phys. Rev. B* 62 (2000) 7365.
- [22] V. Darakchieva, P.P. Paskov, E. Valcheva, T. Paskova, M. Schubert, C. Bundesmann, H. Lu, W.J. Schaff, B. Monemar, *Superlattices and Microstructures* 36 (2004) 573.
- [23] H. Lu, W.J. Schaff, L.F. Eastman, C.E. Stutz, *Appl. Phys. Lett.* 82 (2003) 1736.
- [24] X. Wang, S.-B. Che, Y. Ishitani, A. Yoshikawa, *Appl. Phys. Lett.* 90 (2007) 151901.
- [25] X.M. Duan, C. Stampfl, *Phys. Rev. B* 79 (2009) 035207.